

Boron Nitride Nanotube Peapod under Ultrasonic Velocity Impacts: A Fully Atomistic Molecular Dynamics Investigation

J. M. De Sousa^{a,e,*}, L. D. Machado^b, C. F. Woellner^c, M. Medina^d, P. A. S. Autreto^d, D. S. Galvão^e

^a*Instituto Federal de Educação, Ciência e Tecnologia do Piauí – IFPI, Primavera, São Raimundo Nonato, Piauí, 64770-000, Brazil.*

^b*Departamento de Física Teórica e Experimental, Universidade Federal do Rio Grande do Norte – UFRN, Natal, 59072-970, RN, Brazil.*

^c*Physics Department, Federal University of Parana – UFPR, Curitiba, 81531-980, PR, Brazil.*

^d*Center of Natural Human Science, Federal University of ABC – UFABC, Santo Andre, 09210-580, SP, Brazil.*

^e*Applied Physics Department, State University of Campinas – UNICAMP, Campinas, 13083-859, SP, Brazil.*

Abstract

In this work, we investigated the mechanical response and fracture dynamics of boron nitride nanotubes (BNNTs)-peapods under ultrasonic velocity impacts (from 1 km/s to 6 km/s) against a solid target. BNNT-peapods are BNNTs containing an encapsulated linear arrangement of C₆₀ molecules. We carried out fully atomistic reactive (ReaxFF) molecular dynamics simulations. We have considered the case of horizontal and vertical shootings. Depending on the velocity values we observed tube bending, tube fracture, and C₆₀ ejection. One interesting result was tube unzipping with the formation of bilayer nanoribbons 'incrusted' with C₆₀ molecules.

Keywords: Reactive Molecular Dynamics Method, high strain rate condition, Nanopeapods, Nanopeapod–Boron Nitride Nanotube (BNNT-nanopeapod),

1. Introduction

The hypervelocity impacts (HVI) of single- and double-walled carbon and boron nitride nanotubes have been extensively studied, theoretically and experimentally, in the past decade. In these experiments, the nanotubes collide with solid substrates at ultrasonic velocities (usually between 2 and 8 km/s). Impact forces induce significant deformations that can result in a significant number of new structures, depending on many variables, such as impact angle and velocity, number of layers, material composition, among others^[1–6].

For single-walled carbon nanotubes (SWCNT), the high-velocity impacts generate (due to an internal folding) localized stress on the ends of the tubes, breaking C-C bonds in an almost

*I am corresponding author

Email address: josemoreiradesousa@ifpi.edu.br (J. M. De Sousa)

perfect line, unzipping the SWCNT into carbon nanoribbons^[4]. Similarly, double-walled carbon nanotubes (DWCNT) become completely unzipped (two walls at the same time) through stress accumulation at the edges of the structure, as internal folding is constrained by the second wall^[7]. On the other hand, double-walled boron-nitride nanotubes (DWBNT) unzip one wall at a time, due to the higher hardness of the inner core^[8].

All previously cited studies were carried out for nanotubes in which the external and internal walls have the same compositions (carbon or boron nitride). Experimentally, hybrid tubes with different wall compositions (external and internal) have been already synthesized. One example is the hybrid BN-C nanotube (composed of concentric carbon and boron-nitride walls), experimentally realized by Nakanishi's group^[9]. A study of highly energetic impacts of these new hybrid nanotubes has been already reported, where the authors predicted the elastic response of the individual walls^[10]. The authors showed that they have remarkably different elastic properties in relation to CNT and BNNT. For example, the tubes can decouple, and the carbon nanotube can unzip. These results open up a new perspective for the synthesis of nanostructures with different topologies and compositions.

An interesting example of a hybrid carbon-based nanostructures are the carbon nanotube peapods, which are composed of fullerenes encapsulated into carbon nanotubes. They have been synthesized through different experimental techniques^[11–14], and exhibit very interesting chemical and physical properties^[15–17], and even higher thermal conductivity than SWCNT^[18]. These remarkable properties have been exploited in many applications in nanotechnology, which include transistors^[19], solar cells^[20], nano-memory devices^[21], and supercapacitors^[22]. A previous HVI study^[23] showed that peapods exhibit remarkable resilience under high strain rate conditions. The calculations show large structural deformation and multiple fracture pathways, depending on the impact velocity and relative nanotube-substrate orientation during the impact.

In this work, we investigated another hybrid structure, BNNT-peapods, which are nanostructures composed of C_{60} fullerenes encapsulated into boron nitride nanotubes^[24] (Fig. 1 (a-c)). These structures have been already synthesized by Mickelson et al.^[25].

2. Computational Methodology

In this work, we carried out molecular dynamics (MD) simulations to analyze the fracture patterns of BNNT peapods. We have considered two impact orientations (see Figure 2(a-b)): (a) vertical shooting, where the angle between the BNNT main axis and the plane of the target is 90° ; (b) lateral shooting, where the angle is 0° . For both cases, we considered impact velocity starting from 1 km/s (low speed) up to 6 km/s (ultrasonic speed), with a step velocity increment of 1 km/s. Fully atomistic reactive molecular dynamics simulations were used to characterize the mechanical response of BNNT peapods, their fracture dynamics, and structural deformations under impacts against a rigid target.

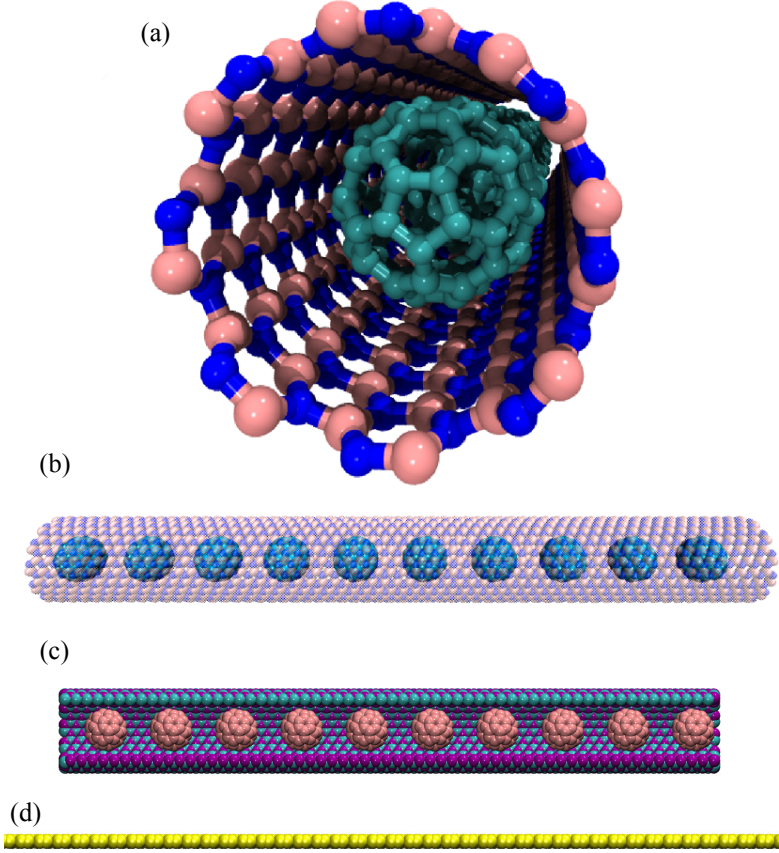


Figure 1: Representative structural atomic model of a boron nitride peapod (BNNT-peapod). (a) Frontal view, and (b-c) side views of a BNNT-peapod with ten encapsulated C₆₀ fullerenes. In (c), part of the outer wall was made transparent for a better view. (d) Side view of the impact target. See text for discussions.

The simulations were carried out using the set of parameters for $H/C/B/N$ atoms defined for the Reactive Force Field (ReaxFF), as implemented in the LAMMPS code^[26]. The reactive force field allows the breaking and formation of chemical bonds, and it was previously used to study the mechanical behavior of nanostructures under ultrasonic impacts^[27–29]. ReaxFF produces results in good agreement with quantum simulation methods in describing carbon-based nanostructures^[30,31].

For all simulations, we considered a 14.9 nm long (12,12) BNNT, containing an encapsulated linear arrangement of 10 C₆₀ molecules. In this configuration, the distance among the C₆₀ is 0.837 nm (see Figs. 2 (a) and (b)). In total, the hybrid system contains 3480 atoms. The target used in the simulations is a rigid van der Waals wall. A time step of 0.025 fs was used to integrate the equations of motion. The BNNT-peapods were first equilibrated in an NVT ensemble at 300 K for 1000 time-steps, using a chain of three Nosé-Hoover thermostats^[32]. Then, we turn off the thermostat, assign a vertical velocity to the system, and let it freely evolve for 5×10^5 time steps in the NVE ensemble. This approach has

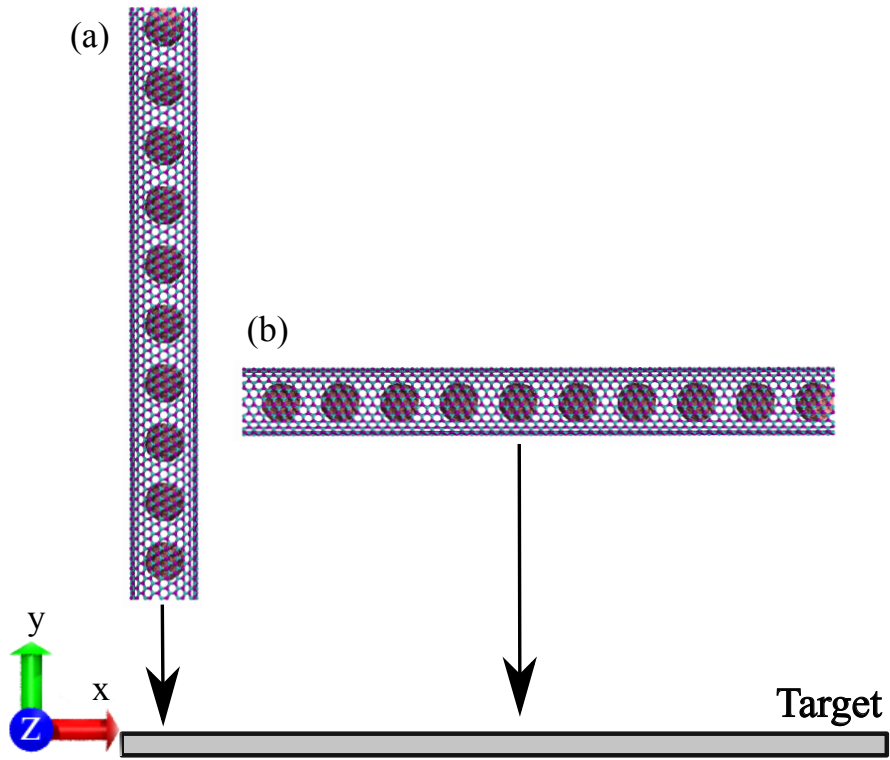


Figure 2: Representative atomic models, showing the considered orientations between the BNNT-peapods and the target substrate. (a) Vertical axis orientation (90° with the target) and (b) lateral axis orientation (0° with the target).

been successfully applied to many theoretical investigations of the hyper-velocity impact of nanostructures^[4,10,28,29].

We analyzed in details the BNNT-Peapods during and after the impacts. During the impact, the BNNT-peapods experience pressure-induced deformations, the pressure values can be evaluated, as a function of time, using the following expression:^[33,34]:

$$P_{atoms} = Nk_B T - \left(\frac{1}{V}\right) \frac{1}{3} \left[\sum_{l=1}^N \sum_{m=1, m>l}^N \left\langle r_{lm} \frac{d\phi}{dr_{lm}} \right\rangle \right]. \quad (1)$$

Where in the first term N is the number of atoms, k_b is the Boltzmann constant, and T is the temperature. The second term is related to the interatomic forces among the atoms, whose elements are the contribution of the force and the position vector components between the l and m atoms in the BNNT peapods. We also calculated the time evolution of the hydrostatic stress, which is equal to one-third of the trace of the stress tensor^[35]. The hydrostatic stress can be negative (for compressive stress) or positive (for tensile stress). A similar methodology was successfully used in other studies^[36–42].

3. Results and Discussions

Representative temporal evolution MD snapshots for vertical shooting (90° degrees with the target) at 3 different speeds (1, 2, and 3 km/s) are presented in Figure 3. The results show that under vertical impact the major structural deformations and/or fractures are on the nanotubes, the degree of these deformations/fractures, as expected, depends on the velocity values. For low values (1 km/s), the conversion of the kinetic energy into elastic energy primarily causes nanotube bending (Figure 3 (a)). As the velocity increases, the tube is fractured, with an increasing number of broken bonds (Figure 3 (b)), resulting in a fast release of the kinetic energy. For $v=2$ km/s, the impact causes both BNNT bending and bond breaking, while for $v=3$ km/s, the impact essentially leads to extensive bond breaking and C₆₀ ejection (Figure 3 (c)). These results are similar to others reported in the literature for tube impact studies showing that the vertical impact can induce extensive fractures due to a high accumulation of energy in a small number of atoms and bonds^[36–42].

Next, we considered the results for horizontal shooting. In Figure 4 are presented some representative MD snapshots for horizontal shooting (0° degree with the target). From this figure, it is possible to see that there is a better distribution the kinetic energy during the impact reducing the number of atoms ejected from the structure. The C₆₀ remain intact for impact velocities up to 3 km/s. For the BNNTs, the level of structural fragmentation again depends on the impact velocity value. For $v=1$ km/s, the nanotube is deformed without fracture, and for $v=2$ km/s, a few bonds break, leading to the formation of defects on the BNNT wall. On the other hand, for $v=3$ km/s, the BNNT fractures are extensive. Careful inspection of the results reveals that bonds break mainly near the C₆₀ inside the nanotubes. We discuss this result in more detail further in the article.

From 4 km/s (Figure 5), the number of broken bonds in the BNNT wall increases, and the impact starts also fracturing the C₆₀. In Figure 6 we present the percentage of broken

bonds as a function of the simulation time, which corroborates this assertion. In this figure, we divided the system into four regions: (i) the bottom and (ii) the top of the BNNT; (iii) the bottom and (iv) the top of the C_{60} . These results reveal a clear relationship between impact velocity and fracture patterns. Examining Figure 6(a), for velocity values equal to or below 3 km/s, there is no predominant region for the fracture of the nanotube. For both, the bottom and top areas, the percentage of broken bonds have a plateau at around 7%. However, as the impact velocity increases, an asymmetry emerges in the bond breakage between the upper and lower regions. For instance, for $v = 5$ km/s, the difference is around 11 percentage points. Thus, for higher impact velocities, the presence of C_{60} induces an increase of broken bonds at the bottom of the nanotubes, preserving the top area. This effect enables the possibility of obtaining graphene nanoribbons from the unzipped nanotubes. For the C_{60} , a similar asymmetry emerges between the top and bottom regions (Figure 6(b)). As mentioned before, for the most part, the fullerenes remain intact after the impact for velocity values below 4 km/s. At $v = 4$ km/s, around 15% of the bonds at the bottom part of the C_{60} breaks, compared to 32% for the BNNT bottom. On the other hand, for an impact velocity of 6 km/s, the C_{60} fractures are more extensive than those of the nanotubes. The C_{60} are almost totally fragmented for this critical velocity value.

BN-peapods at high-velocity impact can also result in unzipped nanotubes. To investigate this possibility, we selected velocity values between 3 km/s (where the asymmetry in bond breakage is small) and 4 km/s (where the fracture is already extensive). The results present below are for a shooting velocity of 3.3 km/s. In Figure 7 we present the hydrostatic stress values as a function of the simulated time. We selected an example where the tube unzipping occurred. To investigate the propagation of stress in detail, we divided the system into four regions and calculated the average stress in each part at each instant. In part (a) of Figure 7, the orange/red curves correspond to the average stress in the lower/upper part of the BNNT, while the gray/black curves correspond to the average stress at the lower/upper part of the C_{60} . One advantage of using the hydrostatic stress is that its sign differentiates compressive (negative) and tensile (positive) stresses. We also analyzed local stress patterns, and in Figures 7(b-e) we used a color scale ranging from red to blue to indicate the local hydrostatic stress values.

Before the collision with the substrate (indicated with the blue dotted line in Figure 7(a)), we find that, as expected, the stress values are low throughout the system (Figure 7(b)). Since the lower part of the BNNT collides first with the substrate, immediately after the impact, the stress increases in this region, leading to the first compressive peak in orange in Figure 7(a). Figure 7(c) presents the corresponding stress distribution in this region, and we find that the entire lower part of the BNNT is under compression at this instant. The stress then propagates upward, towards the lower part of the C_{60} (gray peak in Figure 7(a)) and then towards their upper parts (black peak in Figure 7(a)). Directly after this compressive spike, we notice a sharp tensile stress peak in the upper part of the BNNT, reaching 74.6 GPa, as the C_{60} push this region up (see Figure 7(d)). Consequently, a partial fracture occurs through this BNNT region, as shown in Figure 7 (e). Figure 7(f) provides further insight on the partial unzipping process. In this Figure, we made part of the nanotube transparent to highlight the C_{60} configuration inside the BNNT during the collision. Notice

in the frame obtained at $t = 0.72$ ps that the C_{60} press against the upper part of the BNNT, leading to fracture at some points of contact at $t = 1.10$ ps. In all cases, we only observed partial unzipping as a result of the presence of gaps between the instances. Finally, note that the stress values at the BNNT- C_{60} points of contact are certainly higher than the numbers presented in Figure 7(a)), which provides values averaged over regions of the system.

4. Conclusions and remarks

Fully atomistic reactive molecular dynamics (MD) simulations were carried out to investigate the dynamics of high-velocity ballistic impacts of BNNT-peapods against a solid target for the cases of vertical and horizontal collisions. For low velocity vertical (1 km/s) shootings, the major structural deformations are on the BNNTs (mainly tube bending). Increasing the velocity the tube is fractured with C_{60} ejections. For horizontal shootings, the stress is better distributed and BNNTs retain their structural integrity for small velocity values. Increasing the velocity values, the tube fracture became extensive, with bonds breaking mainly near the encapsulated fullerenes. One interesting result is the formation of nanoribbon structures from unzipped tubes. For instance, for a velocity impact of 3.5 km/s, the BNNT unzips with the formation of a bilayer nanoribbon 'incrusted' with C_{60} .

5. Acknowledgements

This work was supported in part by the Brazilian Agencies CAPES, CNPq (process #310045/2019-3) and FAPESP. J.M.S, M.M. C.F.W, L.D.M., P.A.S.A and D.S.G thank the Center for Computational Engineering and Sciences at Unicamp for financial support through the FAPESP/CEPID Grant #2013/08293-7. JMS acknowledges CENAPAD-SP (Centro Nacional de Alto Desempenho em São Paulo - Universidade Estadual de Campinas - UNICAMP) for the computational support process (proj842).

References

- [1] X. Li, X. Wang, L. Zhang, S. Lee, H. Dai, Chemically derived, ultrasmooth graphene nanoribbon semiconductors, *science* 319 (5867) (2008) 1229–1232.
- [2] L. Jiao, L. Zhang, X. Wang, G. Diankov, H. Dai, Narrow graphene nanoribbons from carbon nanotubes, *Nature* 458 (7240) (2009) 877–880.
- [3] D. V. Kosynkin, A. L. Higginbotham, A. Sinitskii, J. R. Lomeda, A. Dimiev, B. K. Price, J. M. Tour, Longitudinal unzipping of carbon nanotubes to form graphene nanoribbons, *Nature* 458 (7240) (2009) 872–876.
- [4] S. Ozden, P. A. Autreto, C. S. Tiwary, S. Khaliwada, L. Machado, D. S. Galvao, R. Vajtai, E. V. Barrera, P. M. Ajayan, Unzipping carbon nanotubes at high impact, *Nano letters* 14 (7) (2014) 4131–4137.
- [5] S. Ozden, L. D. Machado, C. Tiwary, P. A. Autreto, R. Vajtai, E. V. Barrera, D. S. Galvao, P. M. Ajayan, Ballistic fracturing of carbon nanotubes, *ACS Applied Materials & Interfaces* 8 (37) (2016) 24819–24825.
- [6] L. D. Machado, S. Ozden, C. Tiwary, P. A. Autreto, R. Vajtai, E. V. Barrera, D. S. Galvao, P. M. Ajayan, The structural and dynamical aspects of boron nitride nanotubes under high velocity impacts, *Physical Chemistry Chemical Physics* 18 (22) (2016) 14776–14781.
- [7] R. Dos Santos, E. Perim, P. Autreto, G. Brunetto, D. Galvao, On the unzipping of multiwalled carbon nanotubes, *Nanotechnology* 23 (46) (2012) 465702.
- [8] E. Perim, P. Autreto, R. Paupitz, D. Galvao, Dynamical aspects of the unzipping of multiwalled boron nitride nanotubes, *Physical Chemistry Chemical Physics* 15 (44) (2013) 19147–19150.
- [9] R. Nakanishi, R. Kitaura, J. H. Warner, Y. Yamamoto, S. Arai, Y. Miyata, H. Shinohara, Thin single-wall bn-nanotubes formed inside carbon nanotubes, *Scientific reports* 3 (1) (2013) 1–6.
- [10] E. Armani, P. A. Autreto, High-velocity impact of a hybrid cbn nanotubes, *Oxford Open Materials Science* 1 (1) (2021) itaa006.

- [11] B. W. Smith, M. Monthieux, D. E. Luzzi, Encapsulated c 60 in carbon nanotubes, *Nature* 396 (6709) (1998) 323–324.
- [12] B. Bouteaux, A. Claye, B. W. Smith, M. Monthieux, D. E. Luzzi, J. E. Fischer, Abundance of encapsulated c60 in single-wall carbon nanotubes, *Chemical Physics Letters* 310 (1-2) (1999) 21–24.
- [13] S. Bandow, M. Takizawa, K. Hirahara, M. Yudasaka, S. Iijima, Raman scattering study of double-wall carbon nanotubes derived from the chains of fullerenes in single-wall carbon nanotubes, *Chemical Physics Letters* 337 (1-3) (2001) 48–54.
- [14] B. W. Smith, D. E. Luzzi, Formation mechanism of fullerene peapods and coaxial tubes: a path to large scale synthesis, *Chemical Physics Letters* 321 (1-2) (2000) 169–174.
- [15] H. Muramatsu, T. Hayashi, Y. A. Kim, D. Shimamoto, M. Endo, V. Meunier, B. G. Sumpter, M. Terrones, M. S. Dresselhaus, Bright photoluminescence from the inner tubes of “peapod”-derived double-walled carbon nanotubes, *Small* 5 (23) (2009) 2678–2682.
- [16] R. Pfeiffer, H. Kuzmany, T. Pichler, H. Kataura, Y. Achiba, M. Melle-Franco, F. Zerbetto, Electronic and mechanical coupling between guest and host in carbon peapods, *Physical Review B* 69 (3) (2004) 035404.
- [17] A. Rochefort, Electronic and transport properties of carbon nanotube peapods, *Physical Review B* 67 (11) (2003) 115401.
- [18] E. G. Noya, D. Srivastava, L. A. Chernozatonskii, M. Menon, Thermal conductivity of carbon nanotube peapods, *Physical Review B* 70 (11) (2004) 115416.
- [19] T. Shimada, T. Okazaki, R. Taniguchi, T. Sugai, H. Shinohara, K. Suenaga, Y. Ohno, S. Mizuno, S. Kishimoto, T. Mizutani, Ambipolar field-effect transistor behavior of gd@ c 82 metallofullerene peapods, *Applied physics letters* 81 (21) (2002) 4067–4069.
- [20] R. Hatakeyama, Y. Li, T. Kato, T. Kaneko, Infrared photovoltaic solar cells based on c 60 fullerene encapsulated single-walled carbon nanotubes, *Applied Physics Letters* 97 (1) (2010) 013104.
- [21] C. Lee, K. Kang, K. Park, M. Kim, H. Kim, H. Kim, J. Fischer, A. Johnson, The nano-memory devices of a single wall and peapod structural carbon nanotube field effect transistor, *Japanese journal of applied physics* 42 (8R) (2003) 5392.
- [22] H. Jiang, T. Sun, C. Li, J. Ma, Peapod-like nickel@ mesoporous carbon core-shell nanowires: a novel electrode material for supercapacitors, *RSC advances* 1 (6) (2011) 954–957.
- [23] J. M. De Sousa, C. Woellner, L. Machado, P. Autreto, D. Galvao, Carbon nanotube peapods under high-strain rate conditions: A molecular dynamics investigation, *MRS Advances* 5 (33) (2020) 1723–1730.
- [24] R. Kitaura, H. Shinohara, Endohedral metallofullerenes and nano-peapods, *Japanese journal of applied physics* 46 (3R) (2007) 881.
- [25] W. Mickelson, S. Aloni, W.-Q. Han, J. Cumings, A. Zettl, Packing c60 in boron nitride nanotubes, *Science* 300 (5618) (2003) 467–469.
- [26] S. Plimpton, Fast parallel algorithms for short-range molecular dynamics, *Journal of computational physics* 117 (1) (1995) 1–19.
- [27] R. Paupitz, C. E. Junkermeier, A. C. van Duin, P. S. Branicio, Fullerenes generated from porous structures, *Physical Chemistry Chemical Physics* 16 (46) (2014) 25515–25522.
- [28] J. M. De Sousa, L. D. Machado, C. F. Woellner, P. A. da Silva Autreto, D. S. Galvao, Carbon nanoscrolls at high impacts: A molecular dynamics investigation, *MRS Advances* 1 (20) (2016) 1423–1428.
- [29] C. F. Woellner, L. D. Machado, P. A. Autreto, J. M. De Sousa, D. S. Galvao, Structural transformations of carbon and boron nitride nanoscrolls at high impact collisions, *Physical Chemistry Chemical Physics* 20 (7) (2018) 4911–4916.
- [30] K. D. Nielson, A. C. Van Duin, J. Oxgaard, W.-Q. Deng, W. A. Goddard, Development of the reaxff reactive force field for describing transition metal catalyzed reactions, with application to the initial stages of the catalytic formation of carbon nanotubes, *The Journal of Physical Chemistry A* 109 (3) (2005) 493–499.
- [31] A. C. Van Duin, S. Dasgupta, F. Lorant, W. A. Goddard, Reaxff: a reactive force field for hydrocarbons, *The Journal of Physical Chemistry A* 105 (41) (2001) 9396–9409.
- [32] D. J. Evans, B. L. Holian, The nose–hoover thermostat, *The Journal of chemical physics* 83 (8) (1985)

- 4069–4074.
- [33] M. J. Buehler, Atomistic modeling of materials failure, Springer Science & Business Media, 2008.
 - [34] L. D. Landau, E. M. Lifshitz, et al., Theory of elasticity, Vol. 7, Pergamon Press, Oxford New York, 1986.
 - [35] R. Hill, The mathematical theory of plasticity. oxford univ, Press, London (1950).
 - [36] J. M. De Sousa, T. Botari, E. Perim, R. Bizao, D. S. Galvao, Mechanical and structural properties of graphene-like carbon nitride sheets, RSC advances 6 (80) (2016) 76915–76921.
 - [37] J. M. De Sousa, G. Brunetto, V. R. Coluci, D. S. Galvao, Torsional “superplasticity” of graphyne nanotubes, Carbon 96 (2016) 14–19.
 - [38] J. M. De Sousa, R. Bizao, V. Sousa Filho, A. Aguiar, V. Coluci, N. Pugno, E. Girao, A. Souza Filho, D. Galvao, Elastic properties of graphyne-based nanotubes, Computational materials science 170 (2019) 109153.
 - [39] J. M. De Sousa, P. Autreto, D. Galvão, Hydrogenation dynamics process of single-wall carbon nanotube twisted, Chemical Physics Letters 739 (2020) 136960.
 - [40] J. M. De Sousa, A. Aguiar, E. Girão, A. F. Fonseca, A. Souza Filho, D. Galvão, Computational study of elastic, structural stability and dynamics properties of penta-graphene membrane, Chemical Physics 542 (2021) 111052.
 - [41] W. H. S. Brandão, A. L. Aguiar, L. A. Ribeiro, D. S. Galvão, J. M. De Sousa, On the mechanical properties of popgraphene-based nanotubes: a reactive molecular dynamics study, ChemPhysChem 22 (7) (2021) 701–707.
 - [42] J. M. De Sousa, A. Aguiar, E. Girão, A. F. Fonseca, V. Coluci, D. Galvão, Mechanical properties of single-walled penta-graphene-based nanotubes: A dft and classical molecular dynamics study, Chemical Physics (2021) 111187.

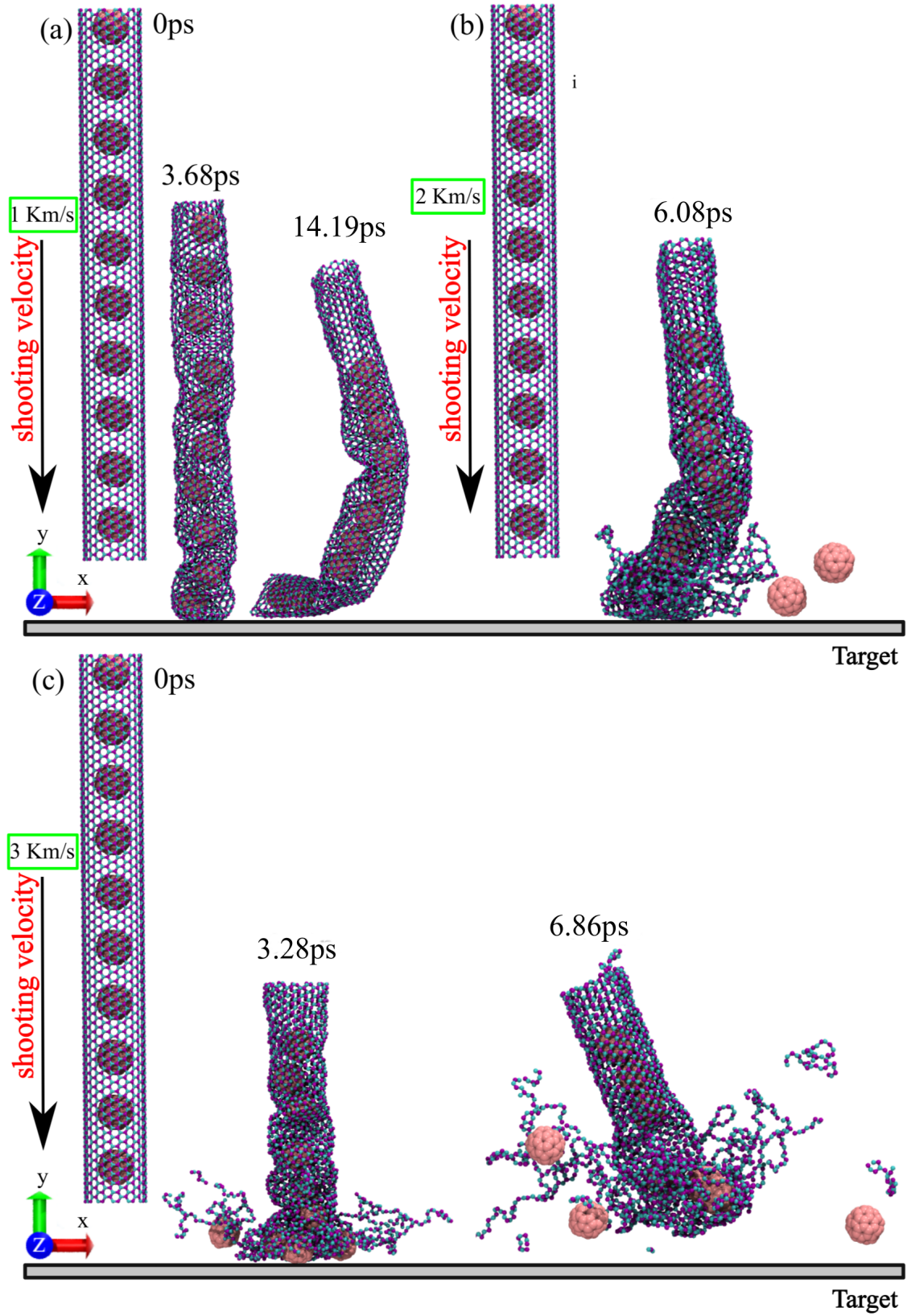


Figure 3: Representative MD snapshots for vertical shooting (90° degrees with the target) at three different impact velocities values. The numbers presented along each snapshot correspond to the time elapsed since the shooting.

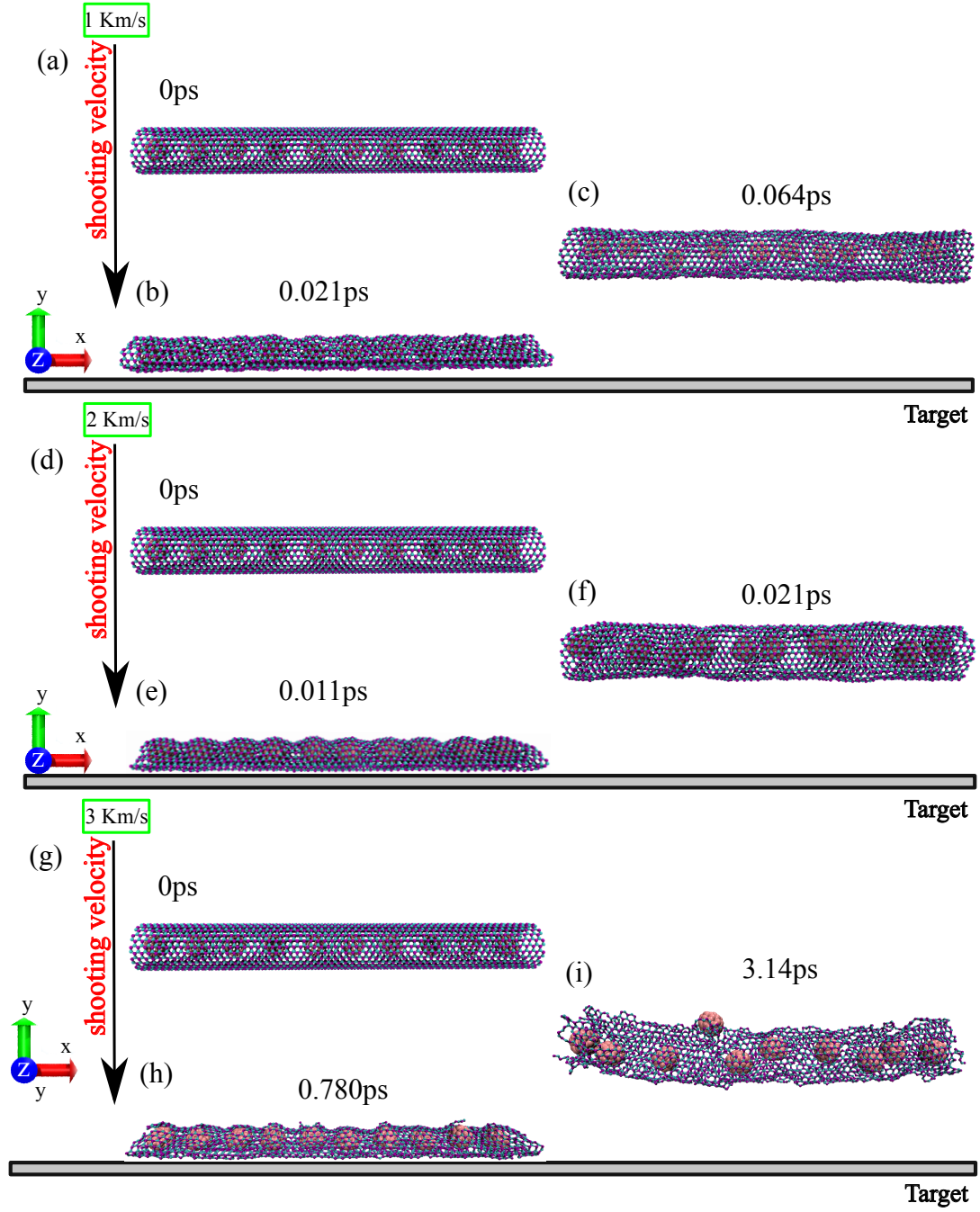


Figure 4: Representative MD snapshots for horizontal shooting (0° degree with target) at three different impact velocity values. The numbers presented along each snapshot correspond to the time elapsed since the shooting.

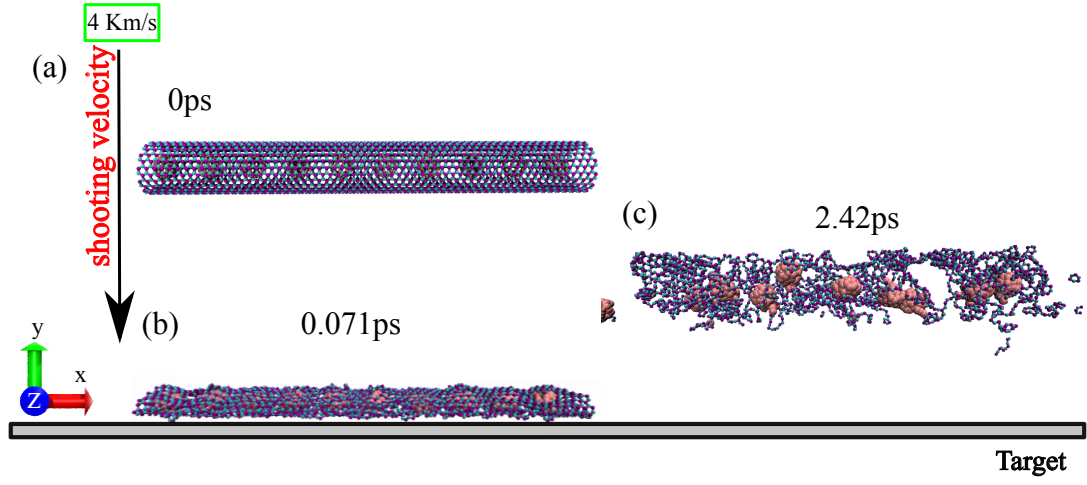


Figure 5: *Representative snapshots for horizontal shooting (0° degree with target) at 4km/s. The numbers presented along each snapshot correspond to the time elapsed since the shooting.*

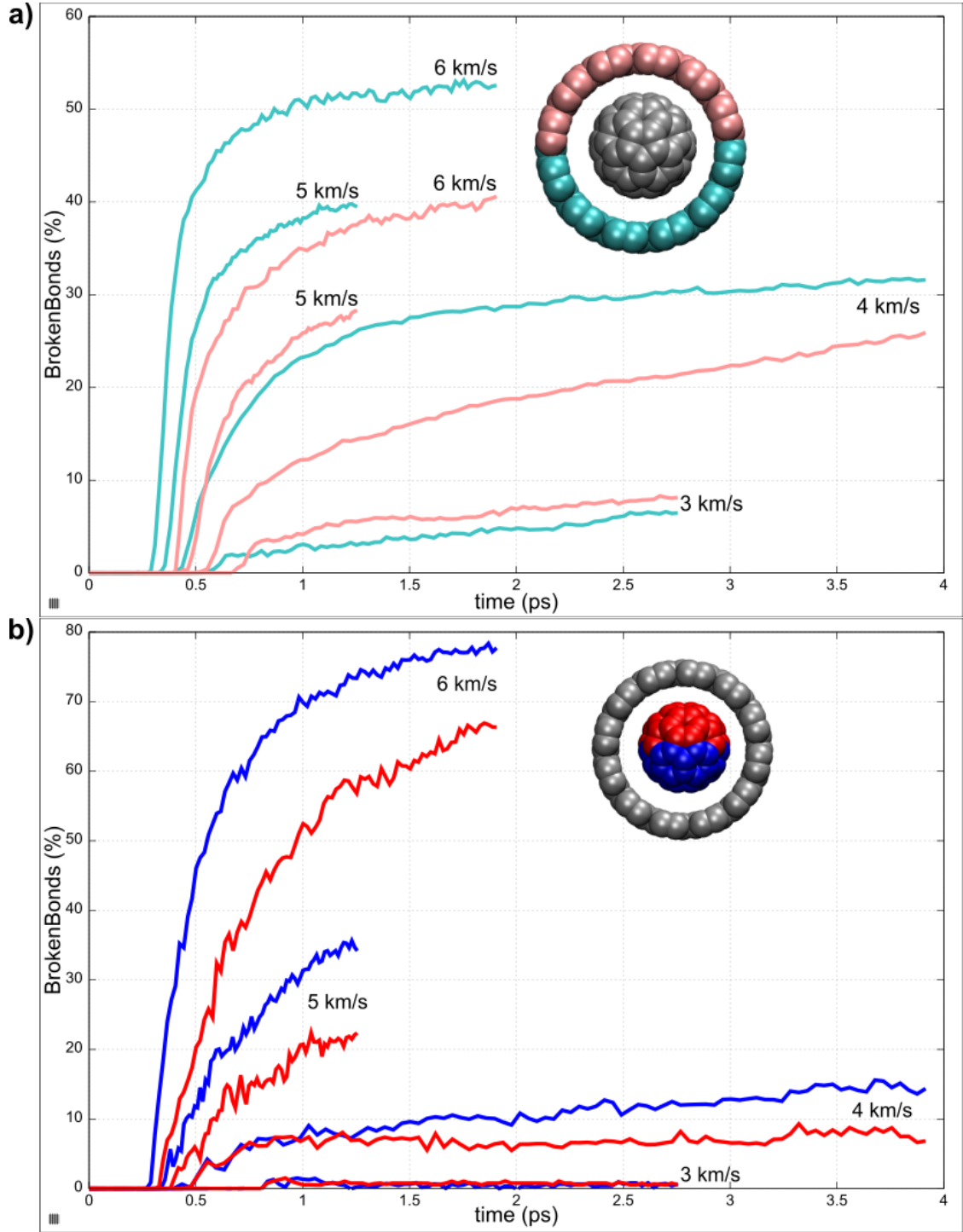


Figure 6: Percentage of broken bonds as a function of the simulation time. (a) Results for the BNNT. The color used to display the curve indicates the corresponding region: pink for the top part and cyan for the bottom one (see the inset). The numbers next to each curve indicate the shooting velocity value. (b) Results for the C₆₀. The color used to display the curve indicates the corresponding region: red for the top part and blue for the bottom one (see the inset).

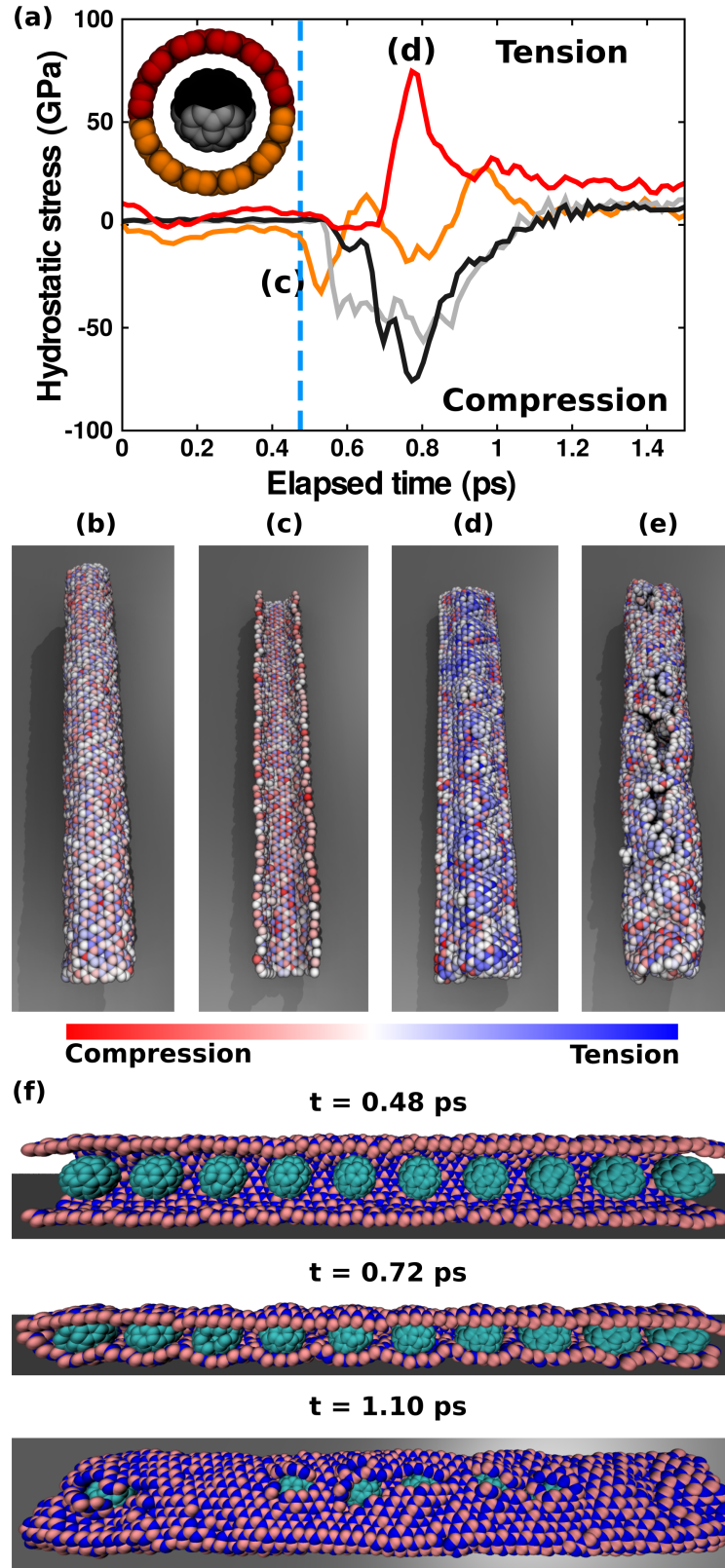


Figure 7: (a) Hydrostatic stress values as a function of the simulation time. Each curve is associated with a corresponding region of the system, illustrated by using the same color in the inset. (b-e) Representative MD snapshots, where the color indicate the local distribution of the hydrostatic stress. (b) and (e) present the initial and final stress configurations, while (c) and (d) present the distribution at the instants highlighted in (a). (f) MD snapshots displaying a side view of the BNNT at three instants, revealing the C₆₀ configuration during the impact.